

We are IntechOpen, the world's leading publisher of Open Access books Built by scientists, for scientists

6,900

Open access books available

186,000

International authors and editors

200M

Downloads

Our authors are among the

154

Countries delivered to

TOP 1%

most cited scientists

12.2%

Contributors from top 500 universities



WEB OF SCIENCE™

Selection of our books indexed in the Book Citation Index
in Web of Science™ Core Collection (BKCI)

Interested in publishing with us?
Contact book.department@intechopen.com

Numbers displayed above are based on latest data collected.
For more information visit www.intechopen.com



Metasurfaces for High Directivity Antenna Applications

Shah Nawaz Burokur, Abdelwaheb Ourir,
André de Lustrac and Riad Yahiaoui
*Institut d'Electronique Fondamentale,
Univ. Paris-Sud, CNRS UMR 8622,
France*

1. Introduction

There has been a lot of study published in literature on the improvement of the performances of microstrip patch antennas. Most of the solutions proposed in the past were to use an array of several antennas. The particular disadvantage of this method comes from the feeding of each antenna and also from the coupling between each element. Other interesting solutions have then been suggested: the first one (Jackson & Alexopoulos, 1985) was to make use of a superstrate of either high permittivity or permeability above the patch antenna and the second one proposed (Nakano et al., 2004), is to sandwich the antenna by dielectric layers of the same permittivity. A Left-Handed Medium (LHM) superstrate where both permittivity and permeability are simultaneously negative has also been suggested (Burokur et al., 2005). The numerical study of a patch antenna where a Left-Handed Medium (LHM) is placed above has been done and in this case a gain enhancement of about 3 dB has been observed. However, these solutions are all based on non-planar designs which are bulky for novel telecommunication systems requiring compact low-profile and environment friendly directive antennas.

To overcome the major problem of complex feeding systems in antenna arrays, the design of compact directive electromagnetic sources based on a single feeding point has become an important and interesting research field. Different interesting solutions based on this concept have been proposed. At first, resonant cavities in one-dimensional (1-D) dielectric photonic crystals have been used (Cheype et al., 2002). Afterwards, three dimensional (3-D) structures have been used, leading to better performances (Temelkuran et al., 2000). Another interesting solution proposed by Enoch *et al.* was to use the refractive properties of a low optical index material interface in order to achieve a directive emission (Enoch et al., 2002). The authors have shown how a simple stack of metallic grids can lead to ultra-refraction. Because the resulting metamaterial structure has an index of refraction, n , which is positive, but near zero, all of the rays emanating from a point source within such a slab of zero index material would refract, by Snell's Law, almost parallel to the normal of every radiating aperture. We shall note that these solutions are all also based on the use of a bulky 3-D material.

Otherwise, the most common method to reach directive emission is obviously based on the Fabry-Pérot reflex-cavity mechanism (Trentini, 1956). Such cavities have first been considered quite bulky too since a thickness of half of the working wavelength is required (Akalin et al., 2002). But recently, the introduction of composite metasurfaces has shown that the half wavelength thickness restriction in a Fabry-Pérot cavity can be judiciously avoided. For example, Feresidis *et al.* showed that a quarter wavelength thick Fabry-Pérot cavity can be designed by using Artificial Magnetic Conductor (AMC) surfaces introducing a zero degree reflection phase shift to incident waves (Feresidis et al., 2005). Assuming no losses and exactly 0° reflection phase, the surface is referred to as a Perfect Magnetic Conductor (PMC), which is the complementary of a Perfect Electric Conductor (PEC). The latter AMC surfaces have been first proposed in order to act as the so called High Impedance Surface (HIS) (Sievenpiper et al., 1999). This HIS is composed of metallic patches periodically organized on a dielectric substrate and shorted to the metallic ground plane with vias, appearing as “mushroom” structures. In a particular frequency band where reflection phase is comprised between -90° and $+90^\circ$, this surface creates image currents and reflections in-phase with the emitting source instead of out of phase reflections as the case of conventional metallic ground plane. The HIS allows also the suppression of surface waves which travel on conventional ground plane. However, the HIS of Sievenpiper needs a non-planar fabrication process, which is not suitable for implementation in lots of microwave and millimetric circuits.

The reflex-cavity antenna proposed by Feresidis was composed of two planar AMC surfaces and a microstrip patch antenna acting as the primary (feeding) source. The first AMC surface was used as the feeding source’s ground plane so as to replace the PEC surface and hence, to achieve a 0° reflection phase. The second one acted as a Partially Reflective Surface (PRS) with a reflection phase equal to 180° . This idea has then been pushed further by Zhou *et al.* (Zhou et al., 2005). By taking advantage of the dispersive characteristics of metamaterials, the authors designed a subwavelength cavity with a thickness smaller than a 10^{th} of the wavelength. Compared to Feresidis, Zhou made use of a non-planar mushroom structure with a dipole acting as the feeding source.

In this chapter, using a novel composite metamaterial, made of both capacitive and inductive grids, we review our recent works in the fields of low-profile and high-gain metamaterial-based reflex-cavity type antennas. First, we will show how our group has lately further reduced the cavity thickness by $\lambda/30$ for applications to ultra-thin directive antennas by using a PEC surface as the source’s ground plane and one subwavelength metamaterial-based composite surface as the PRS. We will also present how an optimization of the cavity has also been undertaken in order to reduce the thickness to $\lambda/60$ by using an AMC surface instead of the PEC ground plane and a metasurface as PRS. We will then present the modeling and characterization of resonant cavities for enhancing the directivity. Finally, a phase controlled metasurface will be proposed for applications to beam steerable and frequency reconfigurable cavity antennas. Numerical analyses using Finite Element Method (FEM) based software *HFSS* and CST’s Transmission Line Modeling (TLM) solver *MICROSTRIPES* together with discussions on the fabrication process and the experimental results will be presented for the different cavities mentioned above.

2. Operating principle of the Fabry-Pérot reflex-cavity

A cavity antenna is formed by a feeding source placed between two reflecting surfaces as shown in Fig. 1. In this paper, different cavities based on the schematic model presented in Fig. 1 will be discussed and used. The cavity is composed of a PEC surface acting as a conventional ground plane for the feeding source and a metamaterial-based surface (metasurface) playing the role of a transmitting window known as a PRS. Following the earlier work of Trentini, a simple optical ray model can be used to describe the resonant cavity modes (Trentini, 1956). This model is used to theoretically predict the operating mode of a low-profile high-directivity metamaterial-based subwavelength reflex-cavity antenna. Let us consider the cavity presented in Fig. 1(a). It is formed by a feeding antenna placed between two reflectors separated by a distance h . Phase shifts are introduced by these two reflectors and also by the path length of the wave travelling inside the cavity. With the multiple reflections of the wave emitted by the antenna, a resonance is achieved when the reflected waves are in phase after one cavity roundtrip. The resonance condition, for waves propagating vertically, can then be written as:

$$h + t\sqrt{\varepsilon_r} = (\phi_{\text{PRS}} + \phi_r) \frac{\lambda}{4\pi} \pm N \frac{\lambda}{2} \quad (1)$$

where ϕ_{PRS} is the reflection phase of the PRS reflector, ϕ_r is the reflection phase of the feeding source's ground plane, ε_r is the relative permittivity of the substrate supporting the primary source and t is its thickness. N is an integer qualifying the electromagnetic mode of the cavity. If the cavity and the substrate thicknesses t and h are fixed, the resonant wavelength is determined by the sum of the reflection phases $\phi_{\text{PRS}} + \phi_r$ for a fixed N . Conversely, for a given wavelength, the thickness h can be minimized by reducing the total phase shift $\phi_{\text{PRS}} + \phi_r$. The use of metasurfaces answers this purpose since they can exhibit an LC resonance. This resonance helps to have a reflection phase response varying from 180° to -180° , passing through 0° at the resonance frequency. By choosing a desired operating cavity frequency above the metasurface resonance where the reflection phase is negative, the sum $\phi_{\text{PRS}} + \phi_r$ can be very small leading to a very low cavity thickness. Since the reflector near the feeding antenna in Fig. 1(a) is composed of a PEC surface, then ϕ_r will be very close to 180° . On the other side, an AMC ground plane is used in Fig. 1(b) and in such case ϕ_r will show frequency dependent phase characteristics.

Therefore, taking advantage of the phase dispersive characteristics of metasurfaces, we will present several models of reflex-cavity antennas, each designed for a specific task. We will first present a $\lambda/30$ (1 mm @ 10 GHz) thick cavity antenna by using a PRS reflection phase value around -120° . This cavity antenna has a narrow beam profile in both E- and H-planes, producing a directivity of 160 (22 dBi). To further reduce the cavity thickness, we will emphasize on the use of two metasurfaces as illustrated in Fig. 1 (b), one as a PRS reflector and the other one as AMC ground plane of the primary source. The combination of these two metasurfaces, particularly the low phase values above their resonance, allows to design very low profile cavity antennas. For e.g., a $\lambda/60$ thickness has been achieved and the latter cavity presents a directivity of 78 (19 dBi).

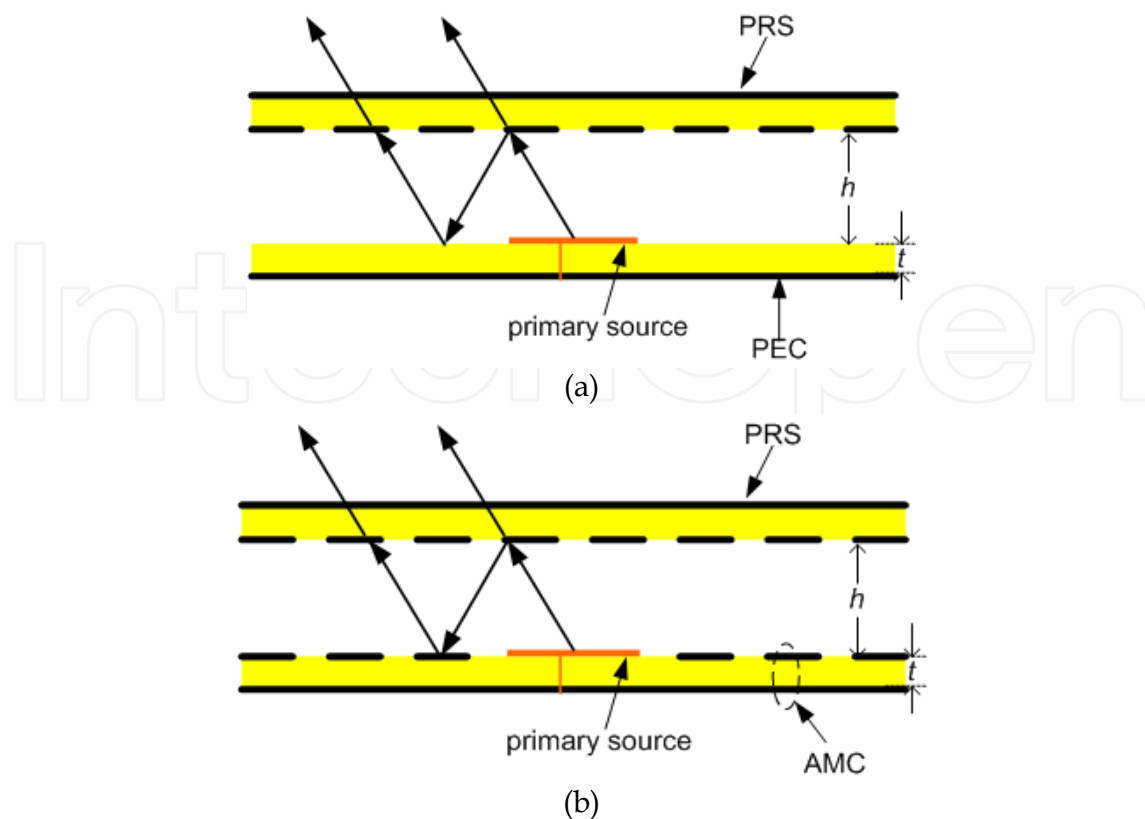


Fig. 1. Resonant cavity formed by a PEC ground plane and a metamaterial-based PRS (a) and, an AMC ground plane and a metamaterial-based PRS (b).

Since directivity depends strongly on the radiating aperture which is defined by the field distribution illuminating the PRS, we will present two ways on how we can manipulate the directivity of such reflex-cavity antennas. First, we will present the use of lateral PEC walls in the cavity antenna to form what we will refer to as metallic cavity. This method allows to enhance the directivity by 3 dB compared to the case where the cavity is open on the lateral sides. Also, the metallic cavity presents lower backward radiations due to the confinement of electromagnetic radiation, therefore increasing the front-to-back (FBR) ratio. Secondly, in order to optimize the field distribution illuminating the PRS, we will study the use of several primary sources inside the cavity. We will show how judiciously placing the different sources in the cavity helps to increase the directivity to more than 6 dB compared to single source fed cavity.

Finally, we will present beam steerable and frequency reconfigurable cavity antennas. For the beam steering, we will in a first step study a cavity where the PRS presents a locally variable phase. The latter PRS then acts as a phased array of micro-antennas, thus allowing to achieve beam steering. This concept has been pushed further by designing an electronically tunable metasurface via the incorporation of lumped elements (varactor diodes). This active metasurface can be used as PRS for two different tasks. Firstly, by applying different bias voltage along the PRS, a locally variable phase is obtained and is fully compatible for beam steering. On the other side, if we change the bias voltage of all the lumped elements similarly, then we can tune the operation frequency of the PRS so as to achieve a frequency reconfigurable reflex-cavity antenna.

3. Analysis of the planar metasurfaces

The cavity presented in Fig. 1 requires the application of a metamaterial-based surface. So in this section, we will design planar metamaterial-based surfaces for operation near 10 GHz.

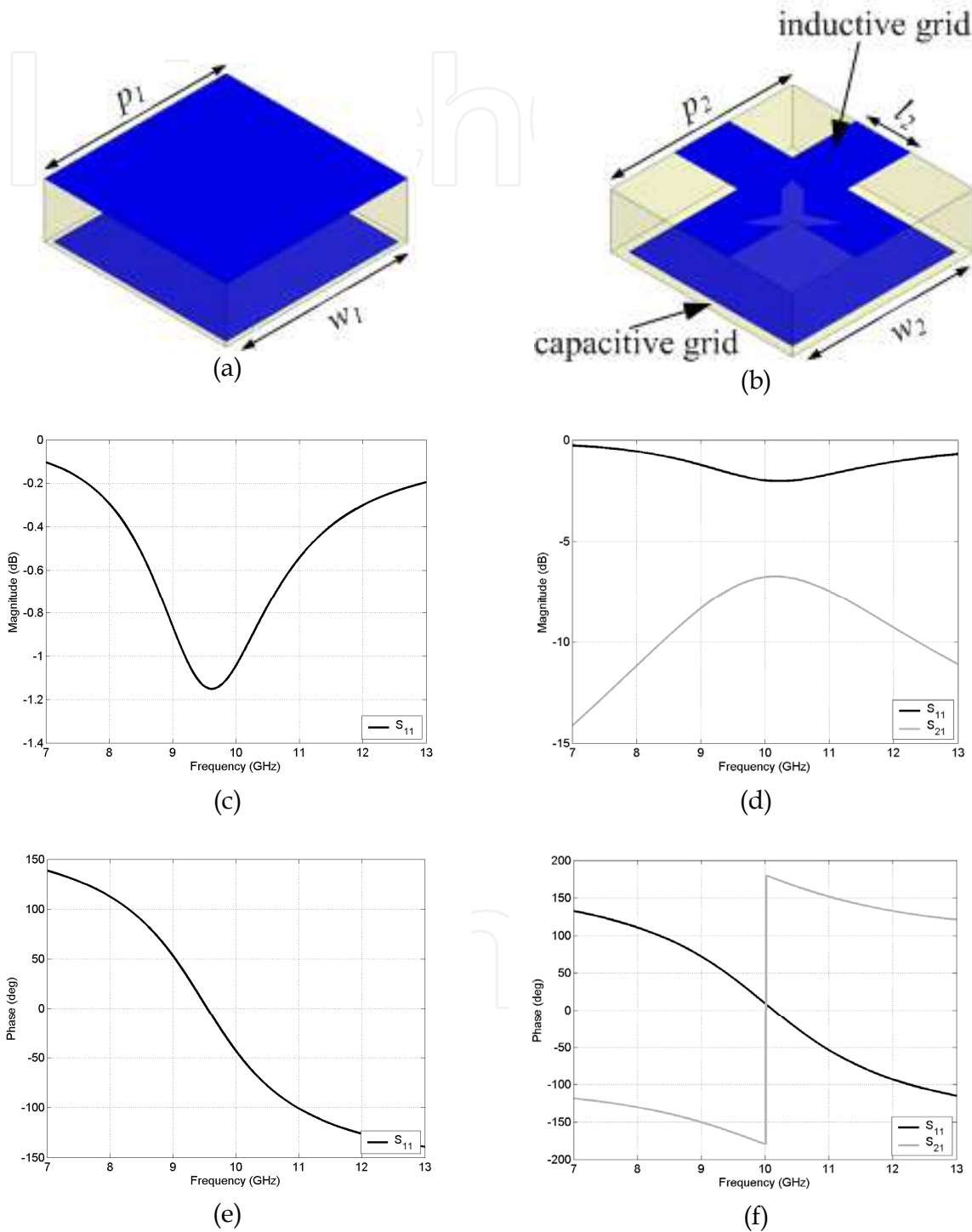


Fig. 2. Unit cell of AMC ground plane (a) and metamaterial-based PRS (b). Calculated reflection magnitude and phase of the AMC ground plane (c), (e) and reflection and transmission magnitudes and phases of the metamaterial-based PRS (d), (f).

The surface used by our group in order to achieve the AMC ground plane is made of a metamaterial composed of 2-D periodically subwavelength metallic square patches organized on one face of a dielectric substrate as illustrated in Fig. 2(a). The different dimensions of the patches are as follows: period $p_1 = 4$ mm and width $w_1 = 3.8$ mm. Another surface which we are going to use for the PRS of the cavity is made of a composite metamaterial consisting of simultaneously a capacitive and an inductive grid on the two faces of a dielectric substrate. The capacitive grid is also formed by 2-D periodic metallic patches (period $p_2 = 4$ mm and width $w_2 = 3.6$ mm) whereas the inductive grid is formed by a 2-D periodic mesh (line width $l_2 = 1.2$ mm) as shown in Fig. 2(b). Concerning the substrate, we have used the double copper cladded epoxy substrate of relative permittivity $\epsilon_r = 3.9$, of tangential loss $\tan\delta = 0.0197$ and having a thickness of 1.2 mm. The size of the different patterns has been chosen in order to minimize the phase of the reflection coefficient near 10 GHz while providing a sufficiently high reflectance (~90%).

The metasurfaces are analyzed numerically using the finite element software *HFSS* so as to present its characteristics in terms of reflection and transmission. Simulations are performed on a unit cell together with appropriate periodic boundary conditions. The results are presented in Fig. 2(c) and Fig. 2(d). As shown, the calculated resonance frequency of the AMC surface and PRS reflector is respectively 10.4 GHz and 9.7 GHz. At resonance, phase crosses 0° as illustrated in Fig. 2(e) and Fig. 2(f).

The composite metamaterial acts as a resonant filter which presents a reflection phase varying from 180° to -180° , depending on the frequency. This variation helps to be more flexible in designing thin cavities by choosing reflection phase values below 0° .

4. Metamaterial-based low-profile highly directive cavity antenna

In this section, we discuss about the design, implementation and characterization of low profile and highly directive cavity antennas. Two different models are presented; an AMC-PRS cavity and a PEC-PRS cavity.

4.1 AMC-PRS cavity antenna

The AMC-PRS cavity antenna is formed by the AMC reflector and the metasurface reflector used as PRS together with a patch antenna designed to operate near 10 GHz (Ourir et al., 2006a). The patch antenna of dimensions 6.8×7 mm² is placed on the AMC in the cavity as shown in Fig. 1(b). The reflectors used are those presented in Fig. 2. The different phases (simulated and measured) are used to estimate the thickness h of the AMC-PRS cavity as given by Eq. (1). Fig. 3(a) shows that h first decreases with increasing frequency of the first resonant mode ($N = 0$) to the point where a cavity zero thickness is reached at around 10.2 GHz. Then a jump in the mode occurs leading to an abrupt variation of h and the value decreases again for $N = 1$. A cavity thickness $h = 0.5$ mm is chosen for the cavity. The thickness h of the Fabry-Perot cavity formed by the two reflectors is adjusted mechanically. The lateral dimensions of the reflector plates are 17×17 cm². This thickness leads to a good matching of the cavity at 10.1 GHz (Fig. 3(b)) corresponding to the design of a $\lambda/60$ cavity. This frequency is in good agreement with the resonance frequency calculated from the optical ray model. The directive emission of the subwavelength cavity antenna at 10.1 GHz

is illustrated from the calculated and measured E-plane ($\phi = 90^\circ$) and H-plane ($\phi = 0^\circ$) radiation patterns in Fig. 3(c) and 3(d).

Using the formulation proposed in (Temelkuran et al., 2000), the directivity of the cavity antenna is written as:

$$D = \frac{4\pi}{\theta_1 \theta_2} \quad (2)$$

where θ_1 and θ_2 are respectively the half-power widths for the E-plane and H-plane radiation patterns. The antenna directivity is then found to be equal to 78 (19 dB) for $\theta_1 = 22^\circ$ and $\theta_2 = 24^\circ$.

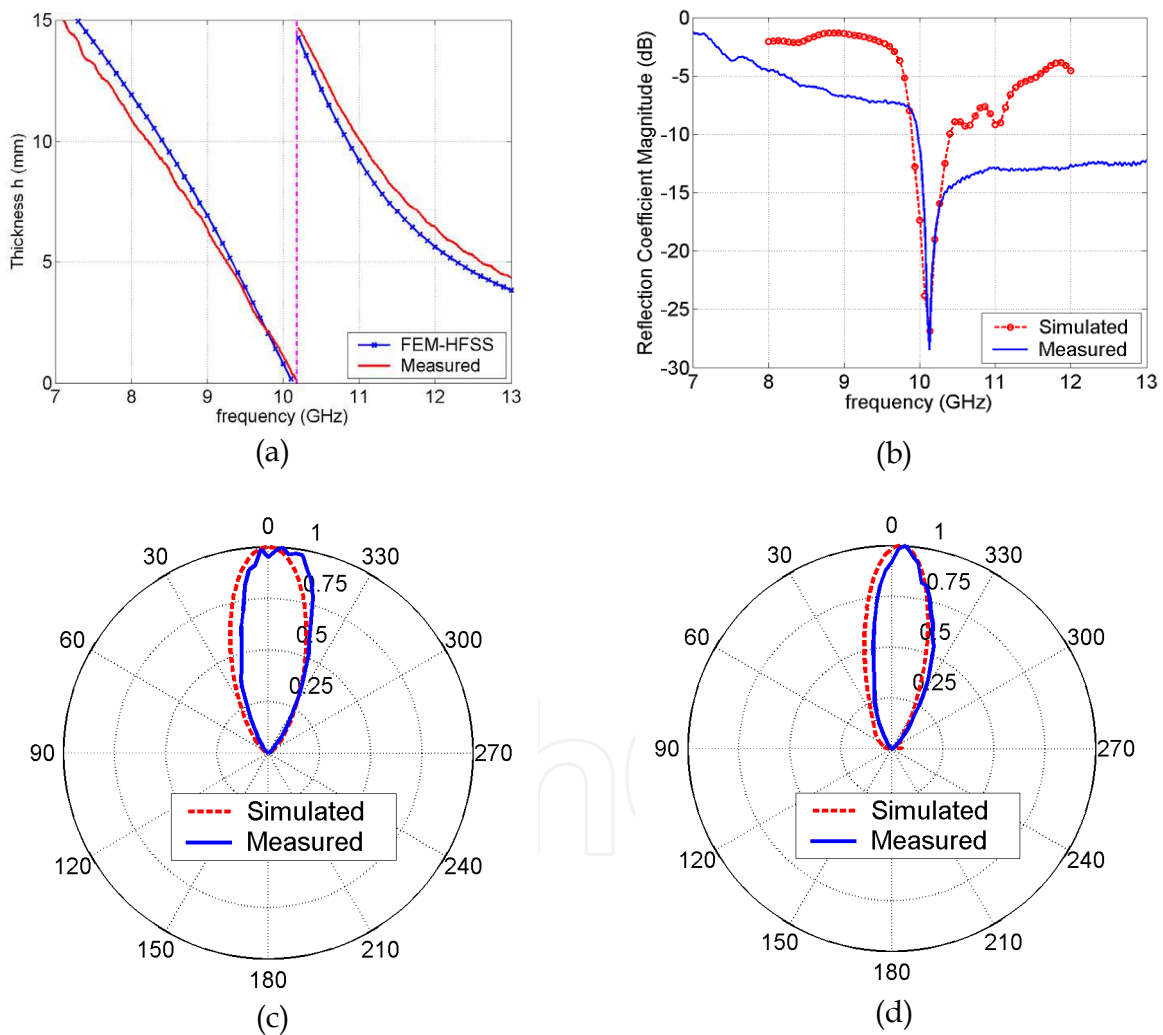


Fig. 3. (a) Evolution of the cavity thickness h versus frequency, this evolution being estimated from Eq. (1) by the calculated and measured reflection phases of the two reflectors used in the AMC-PRS cavity. (b) Calculated and measured matching of the cavity antenna. (c) E-plane ($\phi = 90^\circ$) radiation pattern at 10.1 GHz. (d) H-plane ($\phi = 0^\circ$) radiation pattern at 10.1 GHz.

4.2 PEC-PRS cavity antenna

In order to simplify the fabrication of the cavity antenna, another one using only one metamaterial-based surface reflector acting as the PRS and a PEC reflector (similar to the cavity shown in Fig. 1(a)) is designed (Ourir et al., 2006b). As we have seen from the reflection coefficients in Fig. 2(c) and 2(d), losses are maximum at the resonance frequency of the metamaterial-based surfaces. Thus using only one reflector has also the advantage of presenting lower losses. The PRS composed of simultaneously a capacitive and an inductive grid on the two faces of a dielectric substrate as presented in Fig. 2(b) has been designed for this purpose. Concerning the metallic patches of the capacitive grid, a period $p_2 = 5$ mm and a width $w_2 = 4.8$ mm are used. A line width $l_2 = 2.2$ mm is considered for the mesh of the inductive grid. This PRS having a resonance frequency of about 8 GHz presents a reflection phase close to -150° for frequencies higher than 10 GHz. The use of such a reflector in conjunction with a PEC leads also to a subwavelength cavity since the sum $(\phi_{\text{PRS}} + \phi_t)$ is very close to zero between 9 GHz and 11 GHz.

A 1 mm ($\lambda/30$) thick cavity is designed with lateral dimensions of 10×10 cm² where the resonance is achieved at around 9.7 GHz. The antenna gain patterns in the E- and H-planes obtained from simulation and measurements are presented in Fig. 4(a) and 4(b).

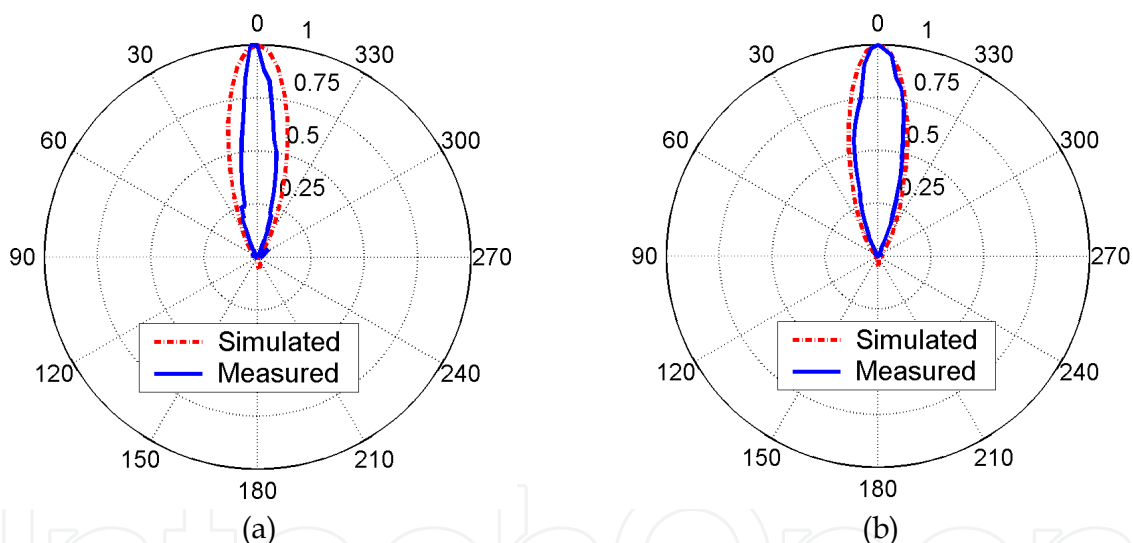


Fig. 4. (a) Calculated and measured reflection phases of the PRS reflector used in the PEC-PRS cavity. (b) Calculated and measured matching of the cavity antenna. (c) E-plane ($\phi = 90^\circ$) radiation pattern at 9.7 GHz. (d) H-plane ($\phi = 0^\circ$) radiation pattern at 9.7 GHz.

In this case, despite the use of only one metamaterial-based surface as the PRS and the use of smaller lateral dimensions than the two metamaterial-based cavity, the antenna directivity is found to be twice and equal to 160 (22 dB).

5. Directivity enhancement in Fabry-Pérot cavity antennas

This section deals with the enhancement of directivity in Fabry-Pérot cavity antennas. Two different approaches are presented to achieve higher performances in terms of directivity and beamwidths. In order to reach a higher directivity, a larger surface of the

PRS must be illuminated. Therefore, a better distribution and confinement of the electromagnetic energy must be produced in the cavity. For this purpose, two innovative solutions can be considered. The first one is to shield the cavity by four metallic walls and the second one is to feed the cavity by multiple primary sources. The two methods are detailed below.

5.1 Metallic cavity antenna

The cavity antenna proposed in this section was designed at 2.46 GHz for point to point radio communication links. The metallic cavity is composed of the feeding antenna's PEC ground plane and a metamaterial-based PRS as reflectors. Furthermore, four metallic walls are also fixed on the lateral sides so as to enhance the directivity of the cavity antenna while keeping low lateral dimensions (Burokur et al., 2009a).

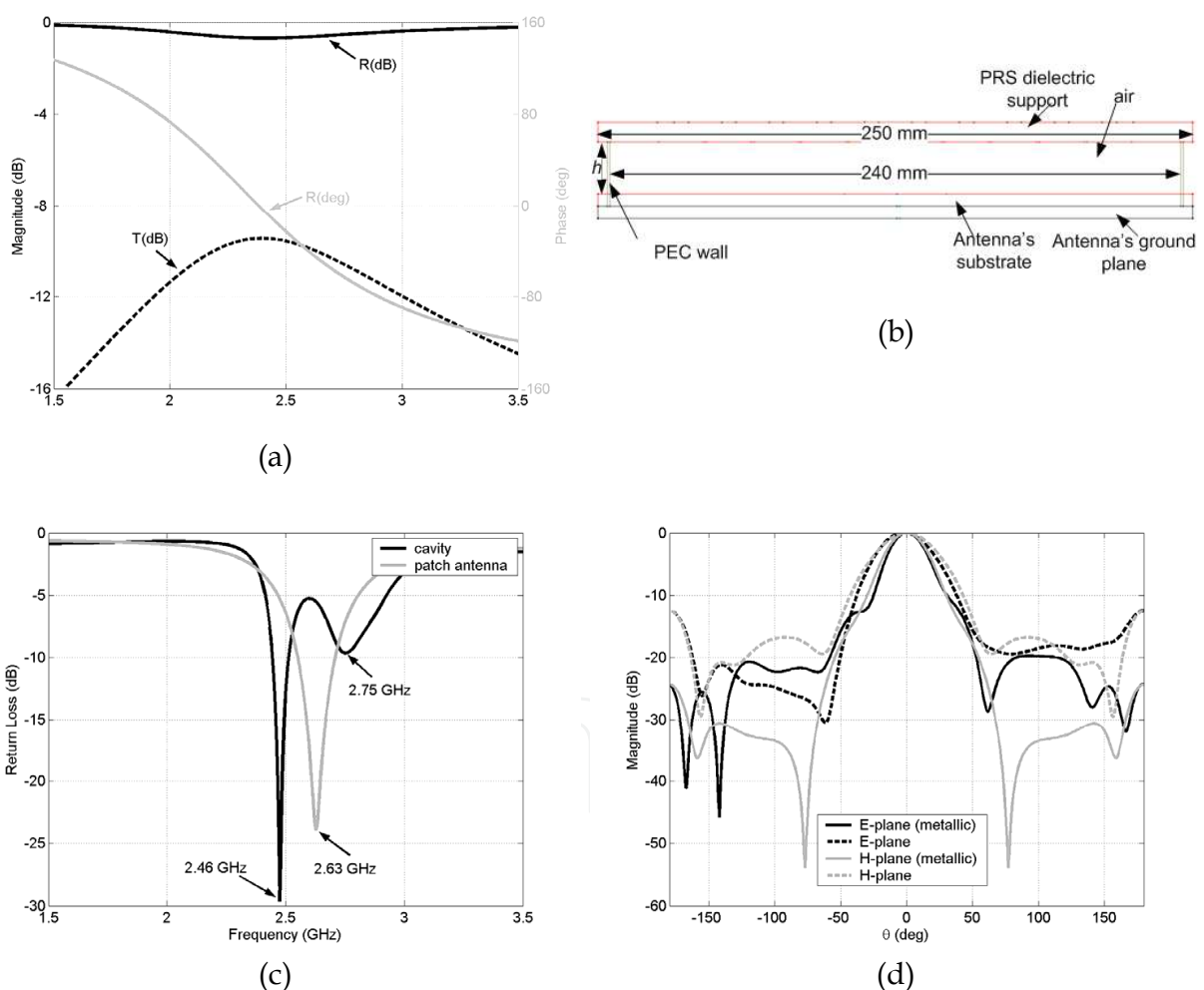


Fig. 5. (a) Calculated reflection phase (solid grey), reflection (solid dark) and transmission (dashed dark) magnitudes for the PRS reflector. (b) Schematic view of the metallic cavity antenna with $h = 21.5$ mm. (c) Return losses of the cavity antenna and the feeding patch antenna. (d) E- ($\phi = 90^\circ$) and H-plane ($\phi = 0^\circ$) radiation patterns at 2.46 GHz for the metallic and conventional cavity antennas.

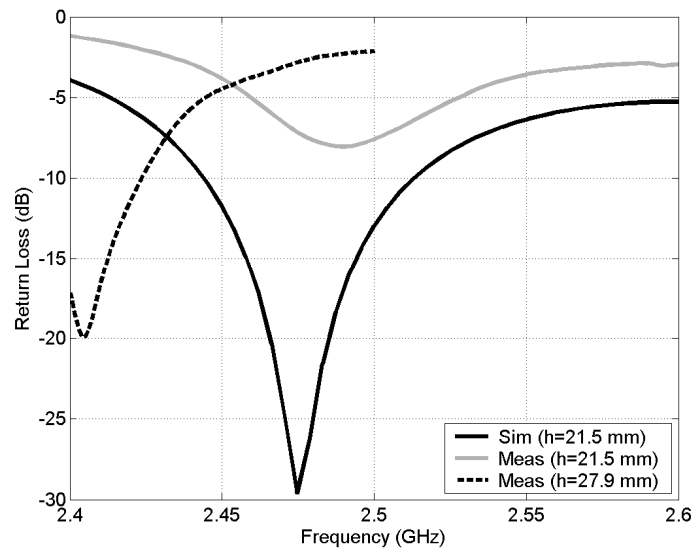
The inductive and capacitive grids of the metasurface are printed on the faces of an 8 mm thick foam dielectric substrate ($\epsilon_r = 1.45$, $\tan\delta = 0.0058$). This thickness is sufficient enough to provide a relatively smooth slope of the phase response, hence rendering the metamaterial less sensitive to fabrication tolerances. The capacitive grid is formed by 2-D periodic metallic patches lattice (period $p_2 = 20$ mm and width $w_2 = 18.8$ mm) whereas the inductive grid is formed by a 2-D periodic mesh (line width $l_2 = 6$ mm). The size of the different patterns has been chosen in order to have the phase of the reflection coefficient below 0° near 2.46 GHz while providing a sufficiently high reflectance ($\sim 90\%$). The numerical results presented in Fig. 5(a) show firstly a resonance frequency of 2.38 GHz, i.e. where the phase crosses 0° . Secondly, we can also note a pass-band behavior where the transmission level is relatively low (about -9.5 dB). Finally this figure shows a reflection phase of -15° at 2.46 GHz.

The microstrip patch feeding source having dimensions 43 mm \times 43 mm is designed on a similar foam dielectric substrate of thickness 5 mm. The surface of the inductive and capacitive grids forming the PRS has dimensions 200 mm \times 200 mm, while the lateral dimensions of the dielectric board supporting the grids as well as that of the cavity have been increased to 250 mm \times 250 mm. However the lateral metallic walls are separated by a distance of 240 mm, as illustrated by the side view of the cavity antenna in Fig. 5(b). So with a $\phi_{\text{PRS}} = -15^\circ$, the thickness of the cavity is found to be $h = 21.5$ mm ($< \lambda/5$). The simulated metallic cavity presents a return loss of 22.8 dB at 2.46 GHz [Fig. 5(c)]. A second resonance is observed at 2.75 GHz corresponding to the resonance of the feeding antenna. These two resonances are situated at each side of that of the feeding patch alone due to the coupling between the patch antenna and the FP cavity.

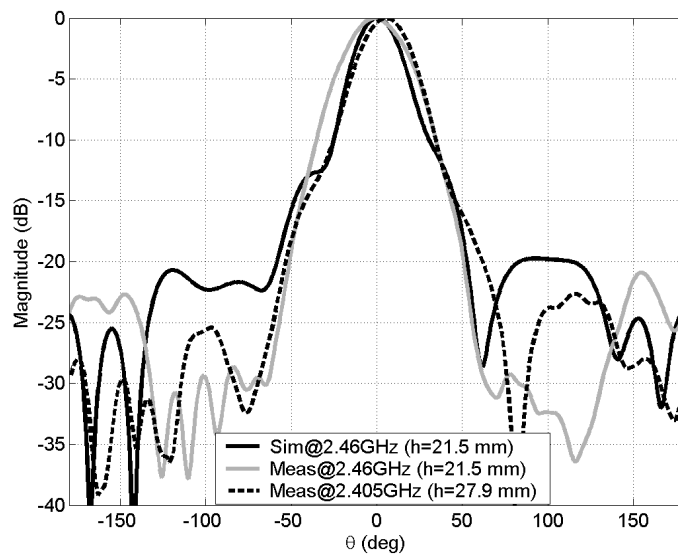
The calculated results [Fig. 5(d)] for the E- and H-plane radiation patterns show a directivity of 15.21 dB. Compared to a similar cavity without metallic walls, an enhancement of about 3 dB and lower secondary lobes are achieved. To reach this same directivity without metallic walls, we should have used a cavity with lateral dimensions close to 400 mm \times 400 mm. Also, the metallic cavity presents very low backward radiations (-24.3 dB) due to the energy confinement by the lateral walls.

A prototype of the proposed cavity has been fabricated and measured (Fig. 6). However, the responses measured with $h = 21.5$ mm have not shown a resonance as expected at 2.46 GHz but at 2.49 GHz. This is due to the matching of the fabricated feeding patch antenna which does not occur at 2.63 GHz as in simulation. Moreover, the responses of the PRS may also present a shift in frequency which can be attributed to the manufacturing tolerances. A modification on the thickness of the cavity has then been undertaken in order to achieve as close as possible the calculated resonance frequency. Three other different thicknesses ($h = 25$ mm, $h = 27.9$ mm and $h = 28.5$ mm) have shown remarkable performances. The different results are summarized in Table 1.

As the thickness increases, the resonance of the cavity antenna tends to lower frequencies. For $h = 25$ mm, the measurements show a return loss of 11 dB and a directivity of 12.79 dB with secondary lobes reaching a level of -26.5 dB. For $h = 28.5$ mm, the return loss is enhanced to 21.5 dB at 2.405 GHz but the directivity falls to 12.4 dB. The best directivity (13.4 dB) is observed at 2.405 GHz for $h = 27.9$ mm with secondary lobes level of -22.7 dB.



(a)



(b)

Fig. 6. (a) Measured return loss of the metallic cavity antenna. (b) Comparison between simulated and measured E-plane radiation patterns.

h (mm)	Resonant frequency (GHz)	Return loss (dB)	Directivity (dB)	Secondary lobes level (dB)
21.5 (sim)	2.46	29.5	15.3	-19.7
21.5 (meas)	2.49	8	12.36	-28.7
25 (meas)	2.46	11	12.79	-26.5
27.9 (meas)	2.405	20	13.4	-22.7
28.5 (meas)	2.4	21.5	12.4	-24.4

Table 1. Performances of the metallic cavity antenna.

5.2 Multisource-fed cavity antenna

As stated earlier, the second method to reach higher directivity is based on the use of multiple primary sources in the cavity. Therefore in this section, the cavities operating near 10 GHz are fed with a 2×2 microstrip patch array (Yahiaoui et al. 2009, Burokur et al., 2009b). The four patches with dimensions $W_p = L_p = 7.5$ mm are fed simultaneously via microstrip transmission lines acting as $\lambda/4$ impedance transformers and excited by a 50Ω SMA connector as shown in Fig. 7(a). The inter-element spacing a of the microstrip patch array feed plays an important role in the directivity of the cavity antenna. For this reason, the influence of this latter parameter is studied for a fixed cavity thickness $h = 1.5$ mm. The inter-element spacing a is varied from 0.5λ to 3λ . The return losses of the cavities are plotted in Fig. 7(b). We can note a very good matching (< -10 dB) around 9.25 GHz for the four different cases.

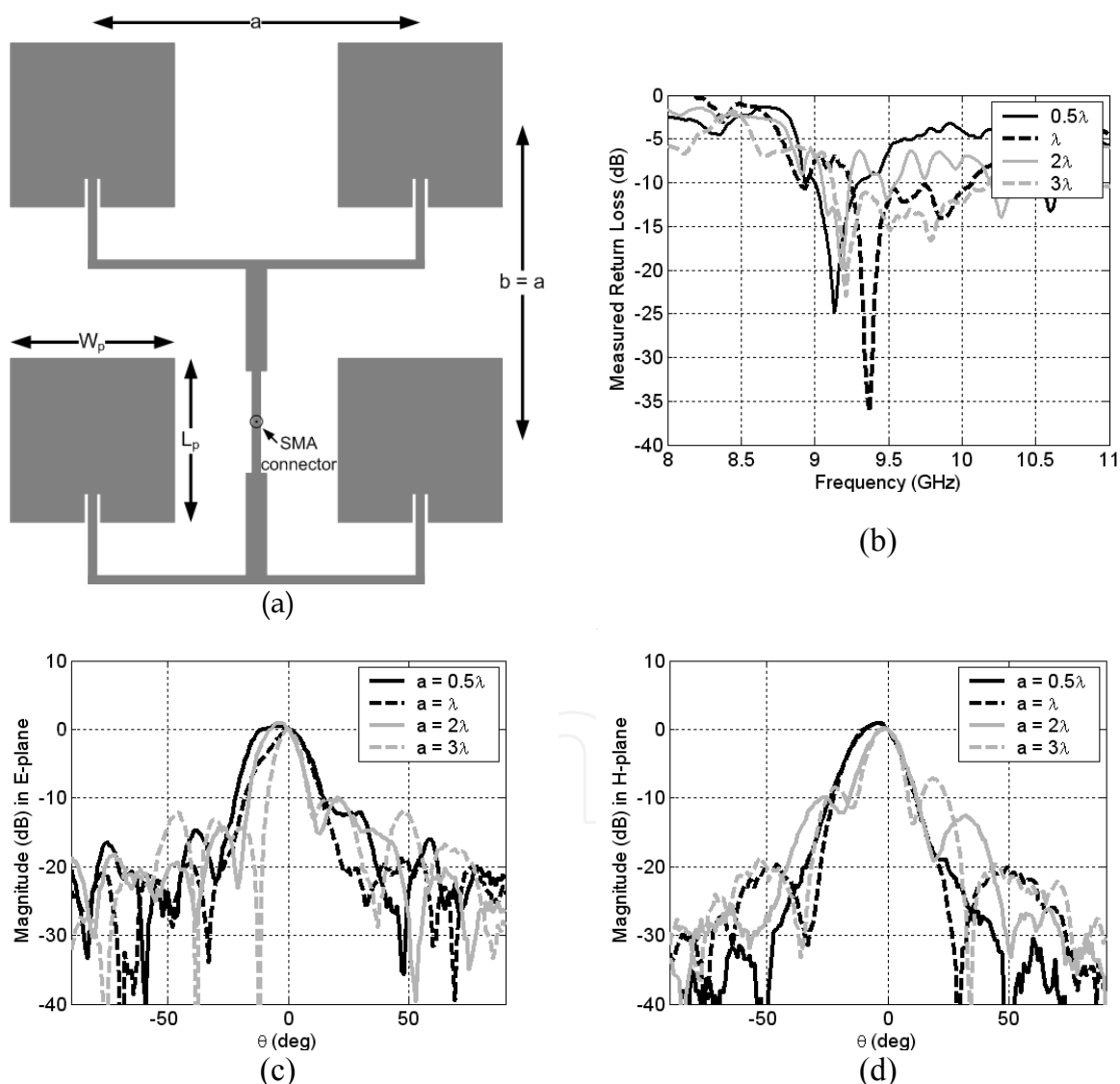


Fig. 7. (a) 2×2 patch array used as a multi-source. (b) Measured return losses of the cavities. (c)-(d) Measured E-plane and H-plane radiation patterns with $a = 0.5\lambda$, λ , 2λ and 3λ for a cavity thickness $h = 1.5$ mm.

The measured E- and H-plane radiation patterns of the cavity antennas are presented in Fig. 7(c) and 7(d). For $a = 0.5\lambda$, a measured directivity of 19 dB is obtained at 8.93 GHz. This value is very close to that of a cavity fed by a single source (see for *e.g.* Ourir et al., 2006a, 2006b). So, it is worth to note that conversely to classical antenna arrays, the directivity is not doubled each time that the number of sources is doubled. For $a = \lambda$, a measured directivity of 20.9 dB is noted at 9.07 GHz, showing clearly an enhancement of 1.9 dB with regard to the case $a = 0.5\lambda$. It is also very important to note that the sidelobes level of the patch array is considerably reduced when embedded in the cavity. This effect is highlighted in Table 2 where the performances of cavities for the different inter-element spacing are presented. 23.21 dB and 25.35 dB is respectively deduced from the measured planes for $a = 2\lambda$ and $a = 3\lambda$. When the case $a = 3\lambda$ is compared to $a = 0.5\lambda$, an increase of 6.35 dB is obtained for the directivity, which is comparable to an increase from a single patch element to a 2×2 patch array. The measured sidelobes level are higher (~ -8 dB in the H-plane) for the case $a = 3\lambda$. However, this sidelobes level is still low compared to the sidelobes level of the source alone. It is well known that an inter-element spacing of an array higher than λ leads to high sidelobes level and also to the apparition of grating lobes.

The directivity D of the cavity antennas can be calculated using $D = 41253/(\theta_1 \times \theta_2)$ where θ_1 and θ_2 are respectively the half-power widths (in degrees) for the H-plane and E-plane patterns. The directivity values are given in Table 2 where we can observe that an increase in the inter-element spacing a in the cavity antenna gives rise to a higher directivity. This is because the radiation area at the surface of the source is bigger when a increases and therefore, a larger surface of the PRS is illuminated by the radiation source. This phenomenon is illustrated in Fig. 8 where the E-field distribution is plotted in a horizontal plane at two different locations z in the cavity antenna. $z = 0$ and $z = 1.5$ corresponds respectively to the plane of the radiating patch array source and to the thickness $h = 1.5$ mm at the inner surface of the PRS (location of the capacitive grid). This figure shows that the radiation area at the surface of the feed source in the case $a = 3\lambda$ is bigger than in the case $a = 0.5\lambda$ and therefore, a larger surface of the PRS is illuminated leading to a higher directivity. On the counter part, the side lobes level also increases.

a (mm)	Resonance frequency (GHz)	Maximum directivity (dB)	Secondary lobes level (dB)
0.5λ	9.13	19 @ 8.93 GHz	-12
λ	9.37	20.9 @ 9.07 GHz	-19
2λ	9.18	23.21 @ 8.94 GHz	-10
3λ	9.21	25.35 @ 8.96 GHz	-8

Table 2. Performances of the cavity antennas with $a = 0.5\lambda$, λ , 2λ and 3λ for a cavity thickness $h = 1.5$ mm.

6. Beam steering in Fabry-Pérot cavity antennas

In this section, we present the modeling and characterization of optimized resonant cavities for beam steering applications. Firstly, the design principle is presented for a passive cavity. The idea is then pushed further to achieve controllable beam steering by incorporating lumped elements in the metasurface reflector.

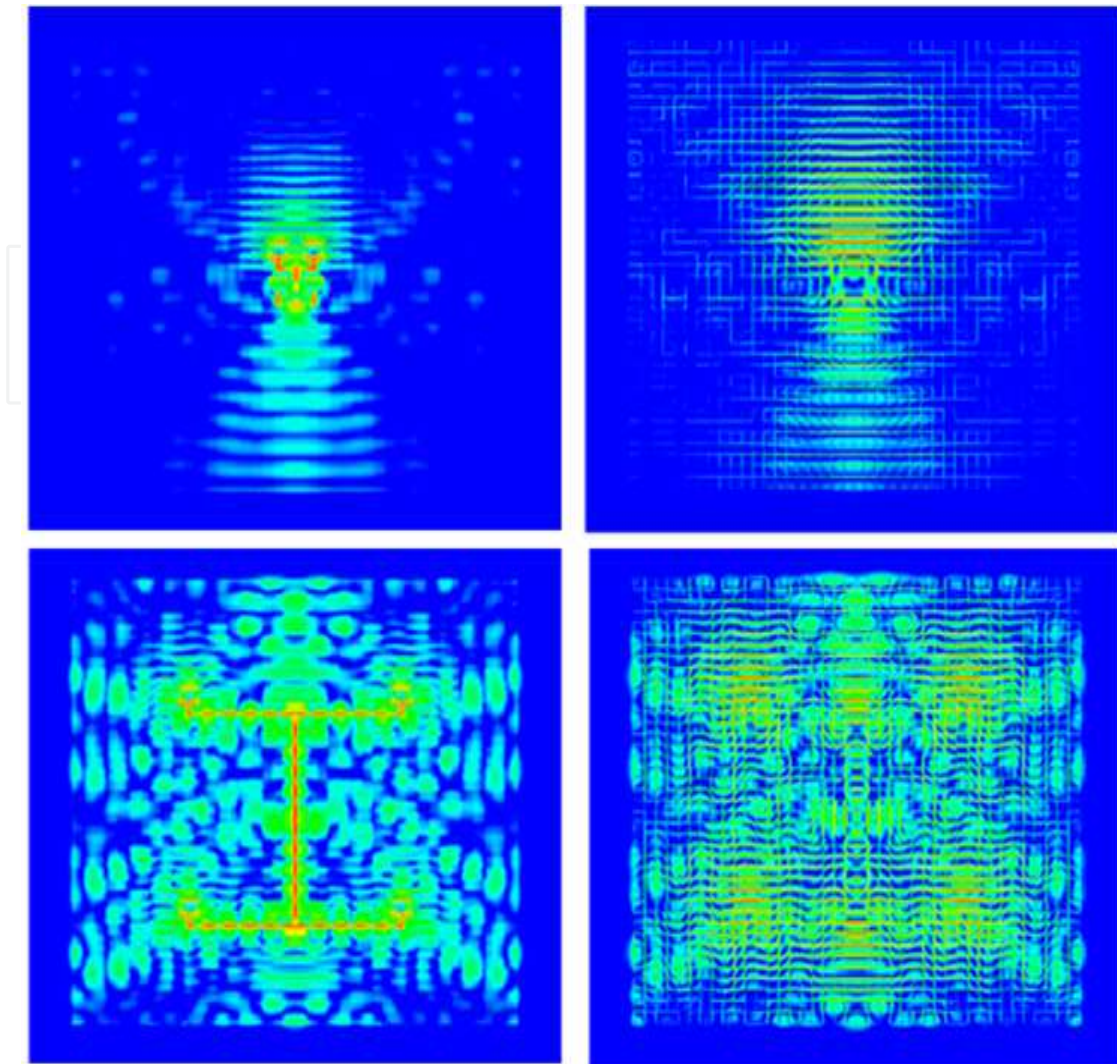


Fig. 8. E-field distribution in a horizontal plane in the cavity antenna for $a = 0.5\lambda$ and $a = 3\lambda$.

6.1 Passive beam steering

Since the beam steering operation is presented in only one radiation plane, the metasurface used is composed of a 1-D array of copper strips etched on each face of a dielectric substrate as shown in Fig. 9(a).

We shall note that the gap spacing g in the capacitive grid plays a crucial role in determining the capacitance and therefore the resonance frequency of the metasurface. By changing g and keeping all the other geometric parameters unchanged, the capacitance of the metamaterial will also vary. As a consequence, the phases of the computed reflection coefficients vary. This behavior is illustrated by the numerical results shown in Fig. 9(b). We can note that the variation of g accounts for the shift of the resonance frequency. An increase in the value of g causes a decrease in the value of the capacitance created between two cells, and finally a shift of the resonance towards higher frequencies. At a particular frequency, the phase of the metasurface increases with an increase in the gap spacing. The study on the variation of g shows that it is possible to design a PRS with a continuous variation of the gap g , resulting in a local variation of the phase characteristics (Fig. 9(c)). If we consider each gap

as a slot antenna, an analogy can then be made with an array of several antennas with a regular phase difference. The locally variable phase metasurface can then be applied for passive beam steering (Ourir et al. 2007a, 2009).

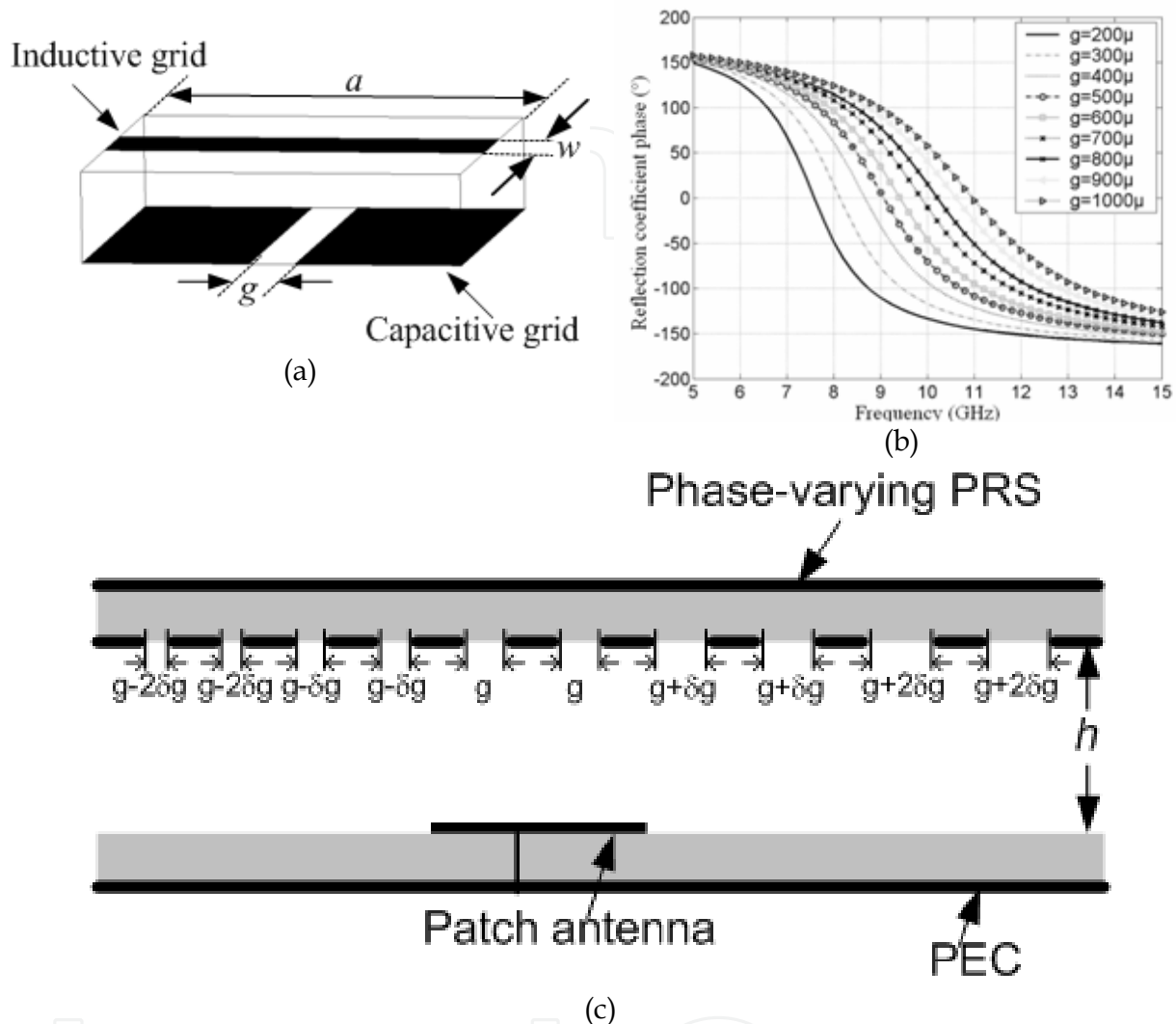


Fig. 9. (a) Elementary cell of the metamaterial composed of an inductive and capacitive grid, which is proposed for the PRS. (b) Reflection phase coefficient of the metasurface versus the gap width g . (c) Schematic view of the cavity composed of a PEC and a metasurface with a variable gap width.

To show the performances in terms of beam steering, several subwavelength cavities have been simulated and fabricated using the 1-D metasurface as PRS. The first one consists of the metamaterial PRS with the same gap spacing $g = 400 \mu\text{m}$ between the metallic strips of the capacitive grid ($\delta g = 0$). This prototype will assure no deflection of the beam since it exists no phase variation of the metamaterial. The second and third ones are the prototypes incorporating respectively a variation of $\delta g = 50 \mu\text{m}$ and $\delta g = 100 \mu\text{m}$ along the positive x -direction. The cases where the variation δg is negative (180° rotation of the PRS around the z -axis) have also been considered. Note that here the resonance frequency of the central region of the metamaterial corresponds to that of the PRS without gap spacing

variation ($g = 400 \mu\text{m}$ and $\delta g = 0$), i.e. 8.7 GHz as shown in Fig. 9(b). The resonance frequency of the cavity is found to be ~ 10.5 GHz for the three prototypes as shown in Fig. 10(a). Best matching is observed when the metallic gap of the PRS capacitive grid increases. However, the resonance frequency remains the same for the three configurations since it depends on the gap spacing of the central region of the PRS, which is the same for the three prototypes.

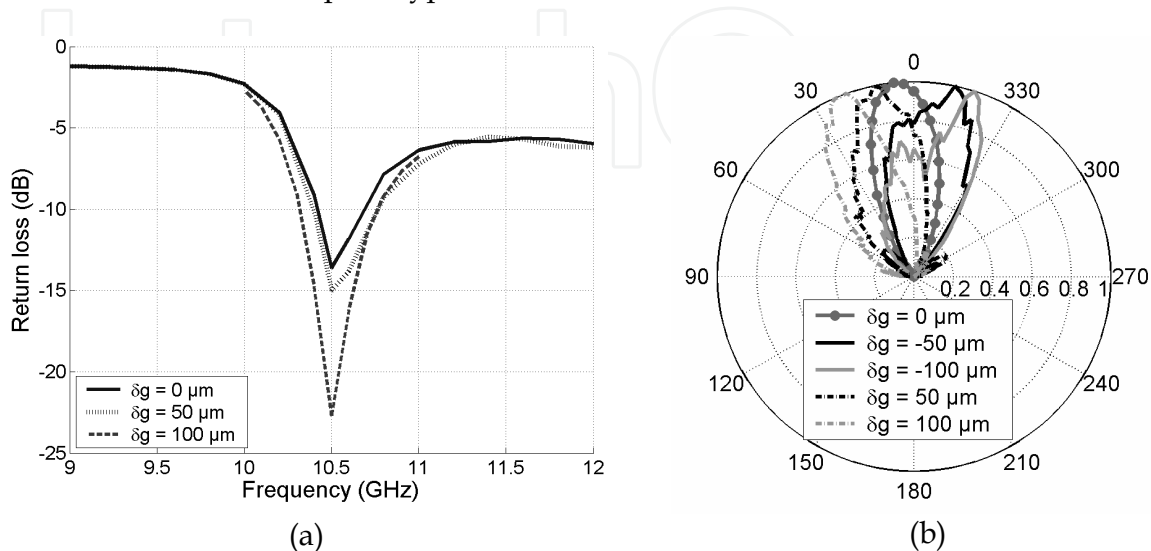


Fig. 10. (a) Return loss of the antennas with different variation of gap width. (b) Measured gain patterns of the cavity antennas versus the gap width variation.

Fig. 10(b) shows the measured gain patterns of the antenna in the E ($\phi = 90^\circ$) plane at 10.5 GHz for an optimized cavity thickness $h = 1$ mm. For $\delta g = 0$, the beam is normal to the plane of the antenna and shows no deflection, which confirms our prediction on the constant phase metamaterial. However, in the case of a regular variation of $50 \mu\text{m}$, a deflection of the antenna beam of about 10° can be observed either in the forward (clockwise) or backward (anti-clockwise) direction depending if δg is respectively negative or positive. Similar observations and a higher deflection of $\pm 20^\circ$ can be noted for $\delta g = \pm 100 \mu\text{m}$. The directivity of the cavity antenna can be calculated using the following expression: $D = 41253/(\theta_1 \times \theta_2)$ where θ_1 and θ_2 are respectively the half-power widths (in degrees) for the H-plane and E-plane patterns. In this case, the directivity is found to be approximately equal to 14.8 dB.

6.2 Active beam steering

The cavity antenna proposed in this section includes the use of lumped elements such as varactor diodes so as to be able to control electronically the phase of the metasurface. As a preliminary step in the design of such cavities, we present firstly the design of the active metasurface.

6.2.1 Electronically controlled metasurface

The metasurface used in this section is based on the same principle as the one illustrated in Fig. 9. But, instead of applying a linear variation of the gap spacing g in order to create a

locally variable phase, we now use active components to make the phase of the metasurface shift in frequency. Varactor diodes having a capacitance value ranging from 0.5 pF to 1.0 pF are thus incorporated into the capacitive grid between two adjacent metallic strips (Fig. 11(a)) and depending on the applied bias voltage, the phase of the metasurface varies with frequency (Ourir et al. 2007b). The variable capacitive grid of the tunable phase PRS used for an operating frequency around 8 GHz consists of a lattice of metallic strips with varactor diodes connected each 6 mm ($s = 6$ mm) between two adjacent strips. The width of the strips and the spacing between two strips of the capacitive grid is respectively $w = 1$ mm and $g = 2$ mm.

Concerning the inductive grid, the width of the strips and the spacing between two strips are respectively $w_1 = 2$ mm and $g_1 = 4$ mm (Fig. 11(b)). Note that the inductive grid is not made tunable. RF chokes are also used in the microstrip circuit in order to prevent high frequency signals going to the DC bias system. Potentiometers are implemented in the structure to create a voltage divider circuit so as to be able to bias locally the varactors. The capacitance in each row can then be adjusted according to the bias voltage applied. This capacitance can also be varied from one row to another by the use of the voltage dividers on the prototype. By changing the bias voltage of the varactors of the PRS similarly, the capacitance of the metamaterial will also vary. As a consequence, the reflection and the transmission coefficients also vary. This behavior is illustrated by the measurement results of the reflection coefficient magnitude and phase shown in Fig. 11(c) and 11(d) respectively. These curves are obtained when the same bias voltage is applied to the different rows of varactors along the PRS. The measurements are performed in an anechoic chamber using two horn antennas working in the [2 GHz - 18 GHz] frequency band and an 8722ES network analyzer. From Fig. 11(c), we can note that the variation of the bias voltage accounts for the shift of the resonance frequency of the PRS, *i.e.* the frequency where the phase crosses 0° . An increase in the bias voltage leads to a decrease in the value of the capacitance of the metamaterial, and finally to a shift of the resonance towards higher frequencies. At a particular frequency the phase of the PRS increases with an increase in the bias voltage. This phase shift is very important since it will help to tune the resonance frequency of the cavity antenna and also to control the radiated beam direction of the antenna.

6.2.2 Active beam steering

Instead of applying a uniform variation in the periodicity of the cells composing the capacitive grid so as to create a locally variable phase as in section 6.1, we now use the electronically controlled metasurface as PRS (Ourir et al. 2009). The active components biased differently make the phase of the PRS shifts in frequency locally. As illustrated by the varactors bias system shown in Fig. 12(a), the proposed PRS is now divided into different regions, where each of them has a specific bias voltage bias. We shall note that here the resonance frequency of the cavity is imposed by the resonance frequency of the central region just above the feeding source corresponding to the bias voltage $V_4 = V_1 + 3\delta V$. The bias voltage is thus increased uniformly with a step δV when moving from the left to the right of the metamaterial-based PRS by the use of the potentiometers. This action creates a regular variation of the phase along the PRS.

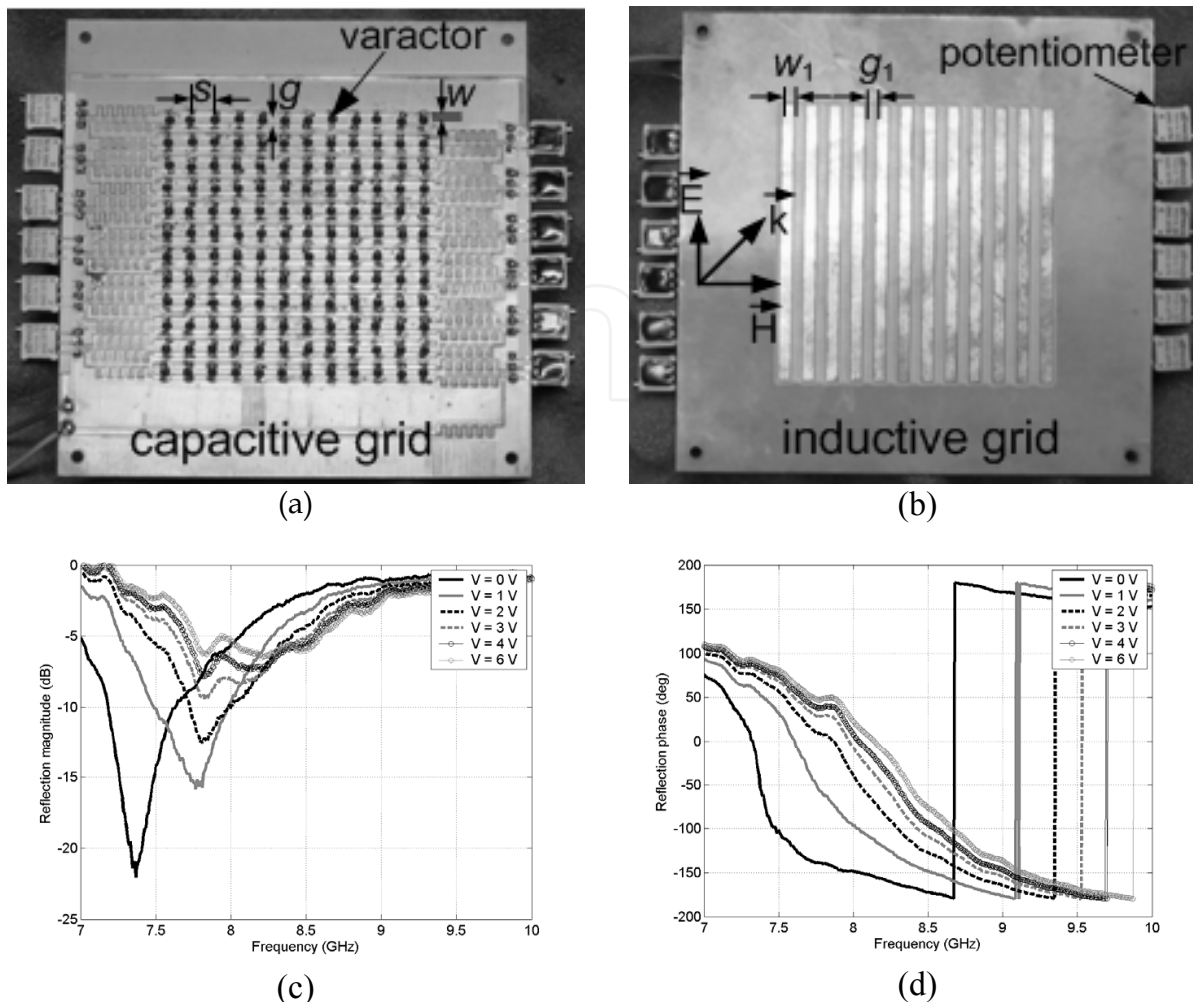


Fig. 11. (a) Electronically phase-varying metasurface. (a) Capacitive grid incorporating varactors and voltage dividers. (b) Inductive grid. (c) Measured magnitude and (d) measured phase of the reflection coefficient versus bias voltage of the varicaps.

The first configuration studied here is the antenna cavity based on the metamaterial PRS with the same null bias voltage for all the varactors. This configuration will assure no deflection of the beam since it exists no phase variation of the metamaterial. The second and third configurations are prototypes incorporating respectively a variation of $\delta V = 0.2$ V and $\delta V = 0.3$ V along the positive x -direction. The cases where the variation δV is negative (180° rotation of the PRS around the z -axis) have also been considered.

Fig. 12(b) shows the gain patterns of the antenna in the E-plane ($\phi = 90^\circ$) at 7.9 GHz for the optimized cavity. For $\delta V = 0$ V, the beam is normal to the plane of the antenna and shows no deflection, which confirms our prediction on the constant phase metamaterial. However, in the case of a regular variation of $\delta V = 0.2$ V, a deflection of the antenna beam of about 7° can be observed either in the forward or backward direction depending if δV is respectively negative or positive. Similar observations and a higher deflection can be noted for respectively $\delta V = 0.3$ V and $\delta V = -0.3$ V. This figure illustrates very clearly the control of the radiation pattern of the antenna by the bias voltage of the varactors. The direction of the radiation beam depends of the direction of the variation of the bias of the varactors. If we

inverse the sign of δV , the sign of the deviation changes also. This demonstration opens the door to the realization of very simple electronically beam steering ultra-compact antennas based on active metamaterials.

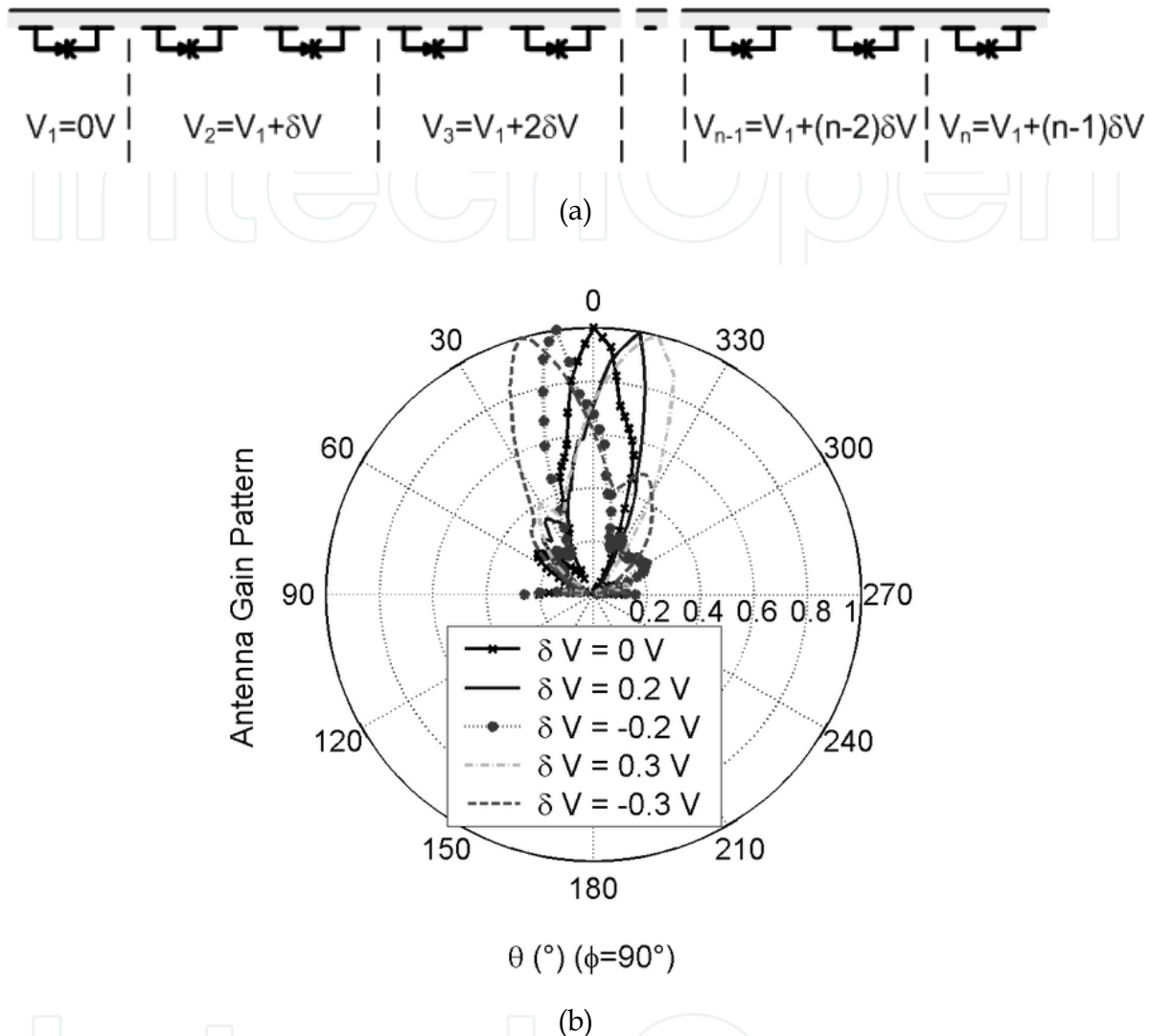


Fig. 12. (a) Variation of the bias voltage of the varactors along the phase varying PRS. (b) Measured gain patterns in the E-plane ($\phi = 90^\circ$) at 7.9 GHz for $\delta V = 0V$, $\delta V = 0.2V$ and $\delta V = 0.3V$. The steering of the antenna's radiated beam can be clearly observed with a positive steering angle for positive bias and negative one for a negative bias.

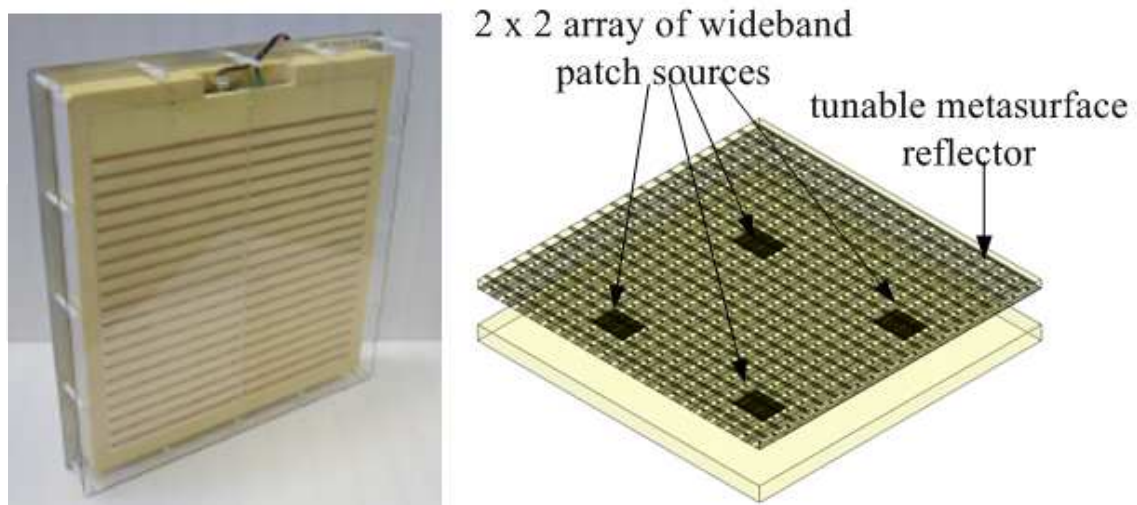
7. Frequency agile Fabry-Pérot cavity antennas

Conversely to beam steerable cavity antennas, we do not need a locally phase-varying PRS for frequency agility applications. What we seek is the ability to change the resonance frequency of the PRS and this is possible by changing simultaneously and in the same manner the capacitance value of the varactor diodes. Here, we show that a tunable metasurface associated to an array of wideband sources in a Fabry-Pérot cavity leads to a reconfigurable directive emission on a wide frequency range (Burokur et al. 2010, 2011). A

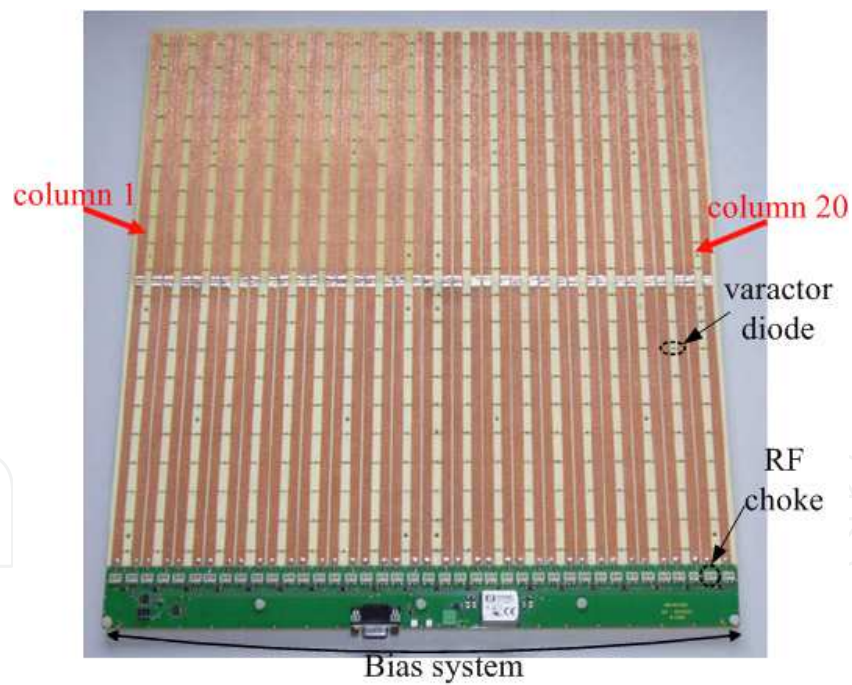
similar electronically controlled PRS as the one shown in Fig. 11(a) is designed to operate near 2 GHz in base station antennas for mobile phone communication systems. The primary source of the cavity is a wideband microstrip patch antenna designed to cover 1.8 GHz – 2.7 GHz frequency range and therefore to illuminate the PRS at any frequency within this range. This patch antenna is electromagnetically coupled to an L-probe which itself is connected to a coaxial connector. Simulations have shown a good matching (return loss < 10 dB) from 1.8 GHz to 2.7 GHz.

To demonstrate experimentally the mechanism for reconfigurable directive emissions from a metamaterial-based FP cavity, a prototype having dimensions 400*400 mm² (approximately $3\lambda \times 3\lambda$) has been fabricated and tested. As it has been shown in section 5.2, the directivity is drastically enhanced when a cavity is fed by judiciously spaced multiple sources since a larger surface of the PRS is illuminated, and therefore the size of the effective radiating aperture of the cavity antenna is increased. Four elementary sources constituting a 2 x 2 wideband patch array are used as primary source; the inter-element spacing between the different sources being 200 mm. Fig. 13(a) and 13(b) shows respectively the photography of the prototype and the capacitive grid of the electronically tunable metasurface. In order to experimentally estimate directivity and gain of the cavity's radiated beam, direct far field measurements are performed using a SATIMO STARLAB and the characteristics are shown in Fig. 14.

When capacitance of the metasurface reflector is changed by varying bias voltage of varactor diodes, the frequency of maximum gain is tuned as clearly shown in the different diagrams of Fig. 14. When 0 V is applied, maximum gain is observed at 1.9 GHz corresponding approximately to the simulated case with $C = 6.5$ pF. When DC bias voltage is increased, the capacitance value is decreased, resulting in an increase of maximum gain frequency. For 24 V, maximum gain occurs at 2.31 GHz, corresponding to lowest capacitance value. To gain more insight in the electromagnetic properties of the metamaterial-based Fabry-Pérot cavity, intensity maps of scanned far field versus frequency and elevation angle θ , in E-plane are presented. The emission frequency represented by the red spot varies from 1.9 GHz to 2.31 GHz from 0 V to 24 V as shown in Figs. 14(a), 14(c), 14(e) and 14(g). These figures demonstrate clearly the frequency reconfigurability property of the cavity. We shall also note that for each frequency the spot is situated at an elevation angle of 0° , indicating a radiated beam normal to the cavity metasurface reflector. Figs. 14(b), 14(d), 14(f) and 14(h) show radiation patterns in E- and H-planes at respectively 1.9 GHz, 2.02 GHz, 2.16 GHz and 2.31 GHz corresponding to maximum gain frequency for 0 V, 5 V, 12 V and 24 V. The tuning range of maximum gain frequency results in an effective operation bandwidth close to 20%. A wide frequency bandwidth is achieved due to the cavity thickness fixed in this particular case. With $h = 15$ mm, reflection phase values around 0° are needed in the 1.85 GHz – 2.25 GHz frequency band. A lower h would lead to phase values approaching -180° and the possible frequency bandwidth from the capacitance tuning range would be narrow. Actually, a high directivity (approximately 18 dBi) is obtained experimentally due to the large lateral dimensions of the fabricated cavity and also to the use of four elementary sources instead of only one where only 14 dBi is obtained.



(a)



(b)

Fig. 13. (a) Photography and perspective view of the cavity antenna. (b) Electronically tunable metasurface reflector incorporating varactor diodes, RF chokes and bias system.

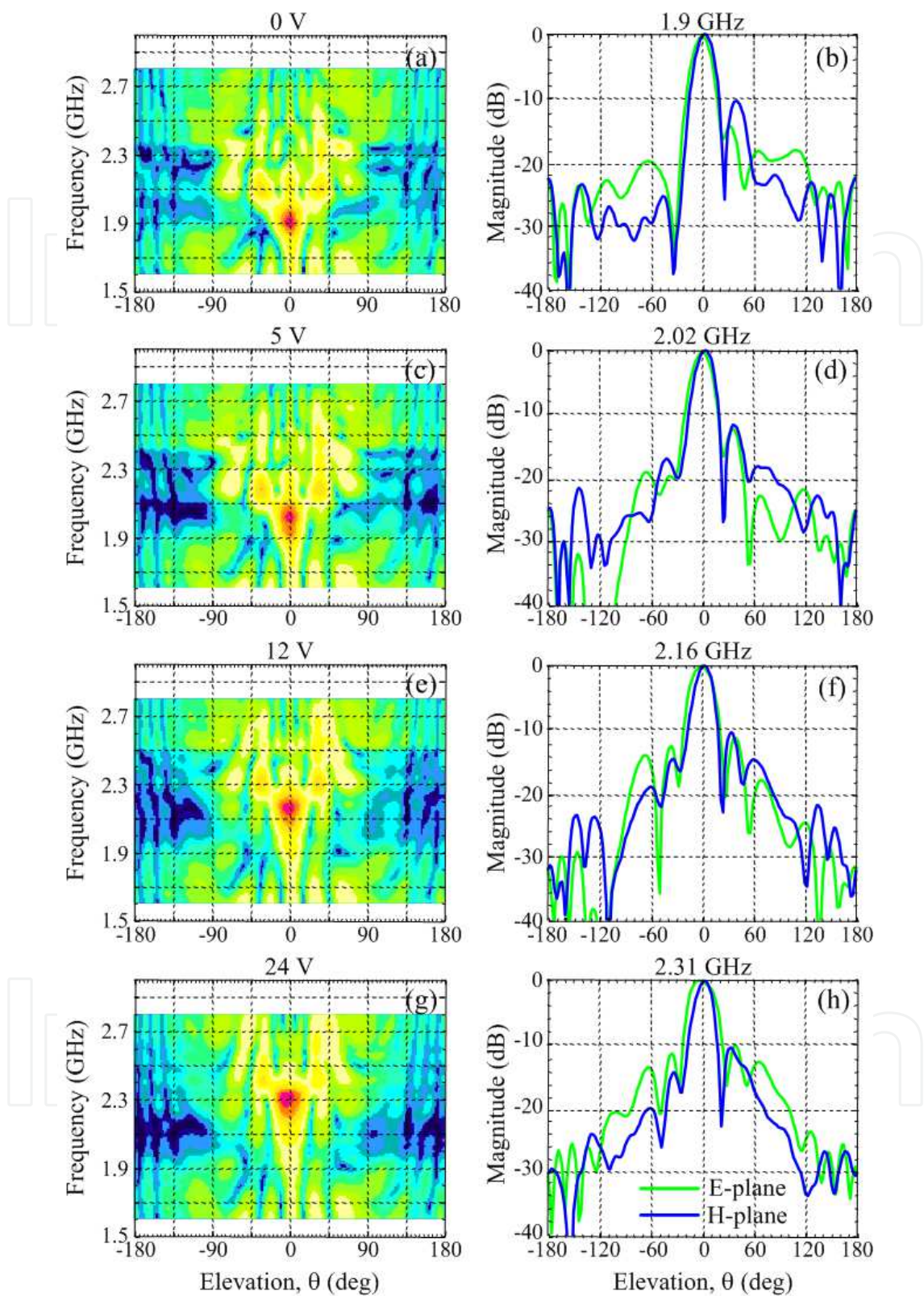


Fig. 14. Far field intensity maps versus frequency and elevation angle in E-plane and measured radiation patterns in E- and H-planes at maximum gain frequency for different bias voltage applied : (a)-(b) 0 V - 1.9 GHz, (c)-(d) 5 V - 2.02 GHz, (e)-(f) 12 V - 2.16 GHz, and (g)-(h) 24 V - 2.31 GHz.

8. Conclusion

To conclude, we have presented various aspects of reflex-cavity antennas: low-profile, high gain, beam steering and frequency agility. For each aspect, numerical calculations together with measurements have been presented. The development of these works has enabled to promote the interesting characteristics of metamaterial-based surfaces. Variable phase metasurfaces compared to conventional PEC and AMC surfaces have also shown their usefulness in reconfigurability applications. Further studies are actually performed to transpose the reflex-cavity antenna concept to industrial applications in various domains such as telecommunications, aeronautical, transport and housing.

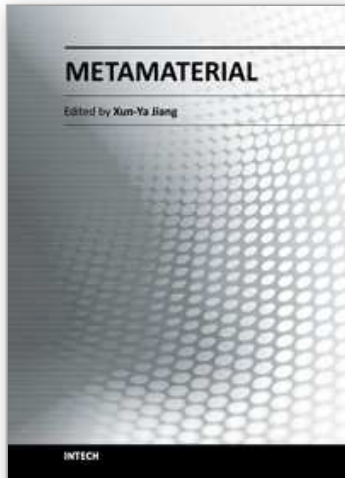
9. Acknowledgements

The authors are very grateful to the French National Research Agency (ANR) for the financial support of the METABIP Project. These works have also been made possible by the partial financial support of the Eureka TELEMAR project. We would like also to thank our partners P. Ratajczak and J.-P. Daniel for the fabrication and characterization of antenna prototypes.

10. References

- Akalin, T., Danglot, J., Vanbesien, O. & Lippens, D. (2002). A highly directive dipole antenna embedded in a Fabry-Perot-type cavity. *IEEE Microw. Wireless Component Lett.*, Vol.12, No.2, (February 2002), pp. 48-50, ISSN 1531-1309.
- Burokur, S.N., Latrach, M. & Toutain, S. (2005). Theoretical investigation of a circular patch antenna in the presence of a Left-Handed Medium. *IEEE Antennas Wireless Propag. Lett.*, Vol.4, (June 2005), pp. 183-186, ISSN 1536-1225.
- Burokur, S.N., Ourir, A., Daniel, J.-P., Ratajczak, P. & de Lustrac, A. (2009a). Highly directive ISM band cavity antenna using a bi-layered metasurface reflector. *Microwave Opt. Technol. Lett.*, Vol.51, No.6, (June 2009), pp. 1393-1396, ISSN 0895-2477.
- Burokur, S.N., Yahiaoui, R. & de Lustrac, A. (2009b). Subwavelength metamaterial-based resonant cavities fed by multiple sources for high directivity. *Microwave Opt. Technol. Lett.*, Vol.51, No.8, (August 2009), pp. 1883-1888, ISSN 0895-2477.
- Burokur, S.N., Daniel, J.-P., Ratajczak, P. & de Lustrac, A. (2010). Tunable bilayered metasurface for frequency reconfigurable directive emissions. *Appl. Phys. Lett.*, Vol.97, No.6, (August 2010), 064101, ISSN 0003-6951.
- Burokur, S.N., Daniel, J.-P., Ratajczak, P. & de Lustrac, A. (2011). Low-profile frequency agile directive antenna based on an active metasurface. *Microwave Opt. Technol. Lett.*, Vol.53, No.10, (October 2011), pp. 2291-2295, ISSN 0895-2477.
- Cheype, C., Serier, C., Thèvenot, M., Monédière, T., Reinex, A. & Jecko, B. (2002). An electromagnetic bandgap resonator antenna. *IEEE Trans. Antennas Propag.*, Vol.50, No.9, (September 2002), pp. 1285-1290, ISSN 0018-926X.
- Enoch, S., Tayeb, G., Sabouroux, P., Guérin, N. & Vincent, P. (2002). A metamaterial for directive emission. *Phys. Rev. Lett.*, Vol.89, No.21, (November 2002), 213902, ISSN 0031-9007.

- Feresidis, A.P., Goussetis, G., Wang, S. & Vardaxoglou, J.C. (2005). Artificial Magnetic Conductor Surfaces and their application to low-profile high-gain planar antennas. *IEEE Trans. Antennas Propag.*, Vol.53, No.1, (January 2005), pp. 209-215, ISSN 0018-926X.
- Jackson, D.R. & Alexópoulos, N.G. (1985). Gain enhancement methods for printed circuit antennas. *IEEE Trans. Antennas Propag.*, Vol.AP-33, No.9, (September 1985), pp. 976-987, ISSN 0018-926X.
- Nakano, H., Ikeda, M., Hitosugi, K. & Yamauchi, J. (2004). A spiral antenna sandwiched by dielectric layers. *IEEE Trans. Antennas Propag.*, Vol.52, No.6, (June 2004), pp. 1417-1423, ISSN 0018-926X.
- Ourir, A., de Lustrac, A. & Lourtioz, J.-M. (2006a). All-metamaterial-based subwavelength cavities ($\lambda/60$) for ultrathin directive antennas. *Appl. Phys. Lett.*, Vol.88, No.8, (February 2006), 084103, ISSN 0003-6951.
- Ourir, A., de Lustrac, A. & Lourtioz, J.-M. (2006b). Optimization of metamaterial based subwavelength cavities for ultracompact directive antennas. *Microwave Opt. Technol. Lett.*, Vol.48, No.12, (December 2006), pp. 2573-2577, ISSN 0895-2477.
- Ourir, A., Burokur, S.N. & de Lustrac, A. (2007a). Phase-varying metamaterial for compact steerable directive antennas. *Electron. Lett.*, Vol.43, No.9, (April 2007), pp. 493-494, ISSN 0013-5194.
- Ourir, A., Burokur, S.N. & de Lustrac, A. (2007b). Electronically reconfigurable metamaterial for compact directive cavity antennas. *Electron. Lett.*, Vol.43, No.13, (June 2007), pp. 698-700, ISSN 0013-5194.
- Ourir, A., Burokur, S.N., Yahiaoui, R. & de Lustrac, A. (2009). Directive metamaterial-based subwavelength resonant cavity antennas - Applications for beam steering. *C. R. Physique*, Vol.10, No.5, (June 2009), pp. 414-422, ISSN 1631-0705.
- Sievenpiper, D., Zhang, L., Broas, R.F.J., Alexópoulos, N.G. & Yablonovitch, E. (1999). High-Impedance Electromagnetic Surfaces with a forbidden frequency band. *IEEE Trans. Microw. Theory Tech.*, Vol.47, No.11, (November 1999), pp. 2059-2074, ISSN 0018-9480.
- Temelkuran, B., Bayindir, M., Ozbay, E., Biswas, R., Sigalas, M.M., Tuttle, G. & Ho, K.M. (2000). Photonic crystal-based resonant antenna with a very high directivity. *J. Appl. Phys.*, Vol.87, No.1, (January 2000), pp. 603-605, ISSN 0021-8979.
- Trentini, G.V. (1956). Partially reflecting sheet arrays. *IRE Trans. Antennas Propag.*, Vol.4, No.4, (October 1956), pp. 666-671, ISSN 0096-1973.
- Yahiaoui, R., Burokur, S.N. & de Lustrac, A. (2009). Enhanced directivity of ultra-thin metamaterial-based cavity antenna fed by multisource. *Electron. Lett.*, Vol.45, No.16, (July 2009), pp. 814-816, ISSN 0013-5194.
- Zhou, L., Li, H., Qin, Y., Wei, Z. & Chan, C.T. (2005). Directive emissions from subwavelength metamaterial-based cavities. *Appl. Phys. Lett.*, Vol.86, No.10, (March 2005), 101101, ISSN 0003-6951.



Metamaterial

Edited by Dr. Xun-Ya Jiang

ISBN 978-953-51-0591-6

Hard cover, 620 pages

Publisher InTech

Published online 16, May, 2012

Published in print edition May, 2012

In-depth analysis of the theory, properties and description of the most potential technological applications of metamaterials for the realization of novel devices such as subwavelength lenses, invisibility cloaks, dipole and reflector antennas, high frequency telecommunications, new designs of bandpass filters, absorbers and concentrators of EM waves etc. In order to create a new devices it is necessary to know the main electrodynamical characteristics of metamaterial structures on the basis of which the device is supposed to be created. The electromagnetic wave scattering surfaces built with metamaterials are primarily based on the ability of metamaterials to control the surrounded electromagnetic fields by varying their permeability and permittivity characteristics. The book covers some solutions for microwave wavelength scales as well as exploitation of nanoscale EM wavelength such as visible specter using recent advances of nanotechnology, for instance in the field of nanowires, nanopolymers, carbon nanotubes and graphene. Metamaterial is suitable for scholars from extremely large scientific domain and therefore given to engineers, scientists, graduates and other interested professionals from photonics to nanoscience and from material science to antenna engineering as a comprehensive reference on this artificial materials of tomorrow.

How to reference

In order to correctly reference this scholarly work, feel free to copy and paste the following:

Shah Nawaz Burokur, Abdelwaheb Ourir, André de Lustrac and Riad Yahiaoui (2012). Metasurfaces for High Directivity Antenna Applications, Metamaterial, Dr. Xun-Ya Jiang (Ed.), ISBN: 978-953-51-0591-6, InTech, Available from: <http://www.intechopen.com/books/metamaterial/metasurfaces-for-high-directivity-antenna-applications>

INTECH
open science | open minds

InTech Europe

University Campus STeP Ri
Slavka Krautzeka 83/A
51000 Rijeka, Croatia
Phone: +385 (51) 770 447
Fax: +385 (51) 686 166
www.intechopen.com

InTech China

Unit 405, Office Block, Hotel Equatorial Shanghai
No.65, Yan An Road (West), Shanghai, 200040, China
中国上海市延安西路65号上海国际贵都大饭店办公楼405单元
Phone: +86-21-62489820
Fax: +86-21-62489821

© 2012 The Author(s). Licensee IntechOpen. This is an open access article distributed under the terms of the [Creative Commons Attribution 3.0 License](#), which permits unrestricted use, distribution, and reproduction in any medium, provided the original work is properly cited.

IntechOpen

IntechOpen